

Continuous Optical 3D Printing of Green Aliphatic Polyurethanes

Sang-Hyun Pyo,^{†,||} Pengrui Wang,^{§,||} Henry H. Hwang,[⊥] Wei Zhu,[⊥] John Warner,[⊥] and Shaochen Chen^{*,§,⊥}

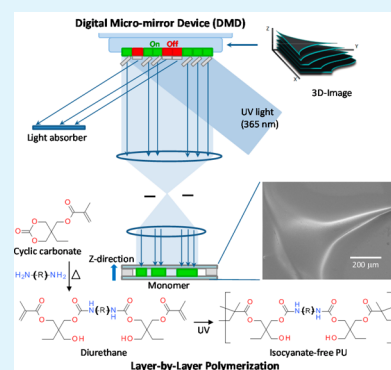
[†]Department of Biotechnology, Center for Chemistry and Chemical Engineering, Lund University, Box 124, 221 00 Lund, Sweden

[§]Materials Science and Engineering and [⊥]Department of NanoEngineering, University of California—San Diego, La Jolla, California 92093, United States

Supporting Information

ABSTRACT: Photosensitive diurethanes were prepared from a green chemistry synthesis pathway based on methacrylate-functionalized six-membered cyclic carbonate and biogenic amines. A continuous optical 3D printing method for the diurethanes was developed to create user-defined gradient stiffness and smooth complex surface microstructures in seconds. The green chemistry-derived polyurethane (gPU) showed high optical transparency, and we demonstrate the ability to tune the material stiffness of the printed structure along a gradient by controlling the exposure time and selecting various amine compounds. High-resolution 3D biomimetic structures with smooth curves and complex contours were printed using our gPU. High cell viability (over 95%) was demonstrated during cytocompatibility testing using C3H 10T1/2 cells seeded directly on the printed structures.

KEYWORDS: 3D printing, continuous optical printing, green polyurethane, gradient stiffness fabrication, biomimicry structure, biocompatibility



1. INTRODUCTION

Biocompatible and nontoxic materials have played an increasingly prominent role in the manufacturing of biomedical devices and the progress of tissue engineering, as the desire to reduce the use of hazardous substances has become a major challenge for human health and environmental consideration.¹ Additionally, the roles of these materials in promoting tissue formation can potentially open new frontiers in the fast-growing field of regenerative medicine;² indeed, the advancement of polymer technologies continues to create polymeric biomaterials that fulfill needs in both medical research and clinical operations alike.³ Naturally derived polymers such as polysaccharides (alginate, chitosan, starch, cellulose, etc.), proteins (collagen, silk, fibroin, etc.), and their derivatives are frequently employed due to their inherent biocompatibility.⁴ However, these naturally derived polymers often do not possess the required physical and mechanical properties required for engineering tissues and organs.⁵ Recently, synthetic polymers such as polyethylene glycol, poly(vinyl alcohol), and polyglycolic acid have been widely investigated due to their flexibility in tuning chemical composition and mechanical properties.^{6–8} However, despite the fact that synthetic polymers often have superior mechanical properties compared to naturally derived polymers, they often still suffer from inadequate strength and durability.^{2,6,8,9}

As a synthetic polymer, polyurethane (PU) is an attractive candidate for medical device applications due to its excellent mechanical strength, flexibility, hydrophobicity, and biocompat-

ibility.⁵ In recent years, biomedical PUs have been developed and incorporated in a variety of biomedical devices.^{5,10–13} However, most PUs are produced by reaction of polyols with isocyanates, and these isocyanates are commonly derived from reacting amines with highly toxic phosgene compounds.^{14,15} Phosgene toxicity aside, isocyanates alone have been reported as one of the primary causes of occupational asthma worldwide due to their high volatility^{14,16} and their tendency to be converted in vivo into aromatic diamines, which are toxic, as well as carcinogenic and/or mutagenic to humans.^{15,17} These toxic residual compounds, although minuscule in amount, are prone to leaking from PU-based products during their operational lifetime.^{14–18} Efforts have been made to reduce such toxicity, such as recent studies that synthesized PU networks from amino acid-derived polyisocyanates that underwent controlled biodegradation to produce noncytotoxic byproducts.^{5,19} However, these PUs were still synthesized from polyisocyanates obtained by toxic phosgenation of amine-terminated lysine esters, and unreacted polyisocyanates can still remain in final polymer.

Thus, there has been increasing attention and societal pressure to find alternative, nontoxic methods to produce isocyanate-free PUs, especially where toxicity to humans is a concern, such as in medical, culinary, and pediatric

Received: October 1, 2016

Accepted: December 9, 2016

Published: December 9, 2016

products.^{18,20–22} Almost two decades ago, P. Anastas and J. Warner introduced the 12 “Green Chemistry Guidelines” to aid chemists in designing safer products.²³ Previous works in green chemistry had introduced halide-free, catalyst-free, and solvent-free reactions^{24–26} to produce chemicals with high renewability and less toxicity. In recent years, ring-opening polymerization (ROP) has been reported by various research groups as a phosgene- and isocyanate-free synthesis pathway.^{18,22,27,28} ROP of cyclic carbonates with polyamines is one example of a green chemistry process to produce polymers without toxic additives, and recently we reported green chemistry synthesis of six-membered functional cyclic carbonates,^{29,30} which are thermodynamically suitable precursors for the ROP process without involving catalysts.^{18,28,31} Furthermore, these cyclic carbonates could incorporate functional groups, such as methacrylate groups, which can be used to impart different properties. Cyclic carbonates have previously been used as biomaterials to make scaffolds, but those attempts were focused on mostly polycarbonate-based materials.^{32,33} In this work, we demonstrate urethane bonds formed by ROP of cyclic carbonates with biogenic amines: putrescine, cadaverine, spermidine, and spermine. These amines are normally formed by the decarboxylation of amino acids as part of the normal metabolism of microorganisms, plants, and animals—their biogenic origin and continuous excretion by the body’s metabolism mark them as harmless, nontoxic additives to the PU synthesis process.^{34–36}

In terms of applications for 3D printing, there have been attempts to utilize PU as a building material for various research needs. Recently, Park et al. used PU-acrylate to fabricate conformal phase masks, in which the acrylate aliphatic urethane oligomer trimethylolpropane-ethoxylated-(15)-triacylate (TMP(EO)15TA) was used confer the necessary elasticity for PU to function as a conformal mold.³⁷ Additionally, Hsieh et al. used a self-designed fused deposition manufacturing platform to bioprint neural stem cell-laden constructs made of thermo-responsive PU hydrogels.³⁸ However, methods like Park et al.’s and Hsieh et al.’s utilized isocyanate-based oligomers and PUs in conjunction with stamp lithography and nozzle-based extrusion, respectively; toxicity aside, these methods both lack resolution and precision. Hsieh et al.’s nozzle-based printing system shares the common disadvantage among 3D printers of its type, namely, that while they can build larger structures, such as an ear or other cartilaginous parts, they lack fine resolution and contour smoothness due to the size of the nozzle as well as the stepwise movement of their motor controllers.³⁸ It is crucial in 3D printing for biomedical application that surface irregularities be minimized, as they can contribute to undesired structural stresses and flow dysfunction.³⁹ Recently, Tumbleston et al. developed a continuous printing system “CLIP”, which shows promising results for rapid prototyping structures with smooth surfaces.⁴⁰ However, their build material, trimethylolpropane triacylate (TMPTA), is highly toxic and carcinogenic, which severely limits its uses in biomedical applications.⁴¹ To the best of our knowledge, direct continuous optical 3D printing of PUs for biomedical research has not been reported.

In this study, we report for the first time the continuous optical 3D printing of green chemistry-derived, isocyanate-free aliphatic polyurethanes (gPUs). We first synthesized photosensitive diurethane monomers prepared from biogenic amines and six-membered cyclic carbonates functionalized with methacrylate group. This gPU prepolymer is then UV-cross-

linked via our in-house continuous optical printing (COP) technique into 3D constructs with user-defined geometries and mechanical properties, enabling quick, high-resolution, and high-throughput creation of biologically relevant structures. We characterized the physical properties of our gPU structures in terms of transparency, stiffness, thermal behavior, and cell biocompatibility.

2. EXPERIMENTAL SECTION

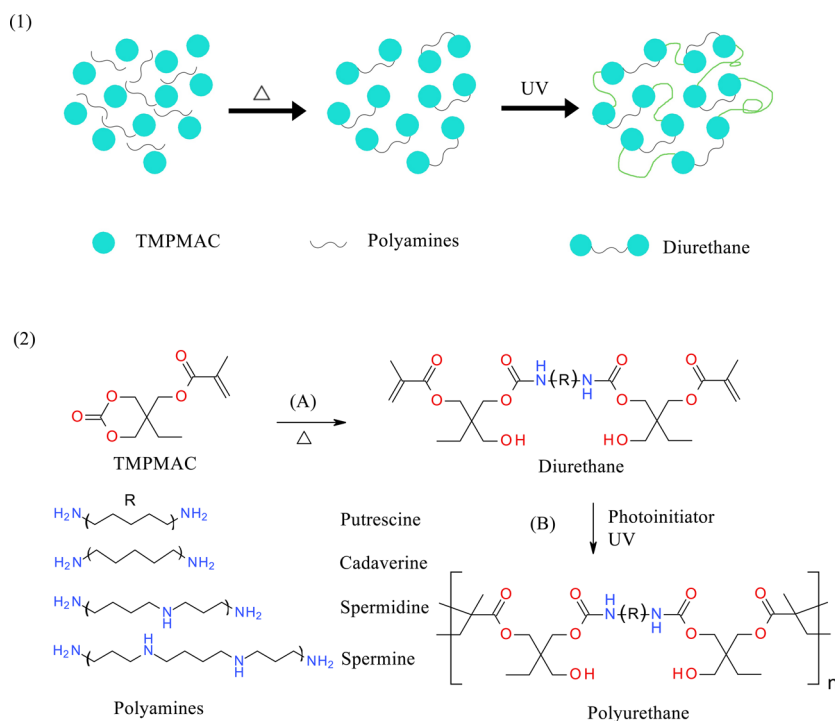
Materials Preparation. Monomethacrylated trimethylolpropane cyclic carbonate and biobased cadaverine and putrescine were kindly provided by Cyclacor AB (Sweden) and CJ Cheiljedang Corp. (South Korea), respectively. Spermine and spermidine were purchased from Sigma-Aldrich. All chemicals were used without further treatment. The photoinitiator (lithium phenyl-2,4,6-trimethylbenzoylphosphine (LAP)) was synthesized according to previous work.⁴² Diurethanes functionalized with methacrylate were prepared from reaction of TMPMAC with diamine compounds such as putrescine, cadaverine, spermidine, and spermine. For example, 1 mmol of TMPMAC was mixed and reacted with 0.5 mmol of cadaverine in a 1.5 mL vial at 70 °C for 10 min without catalysts and solvents. An ethanol and deionized water solution of 3:1 (v/v) ratio was prepared, in which the photoinitiator (LAP) was dissolved to make a photoinitiator solution of 2% (w/v).

Polymerization and 3D Printing. The synthesized diurethane monomers were dissolved in a 1:3 ratio with the photoinitiator solution to make them photopolymerizable. The diurethane solution was injected into a PDMS compartment covered with a glass coverslip chemically modified by 3-(trimethoxysilyl)-propyl methacrylate to provide an anchoring point for the gradient structure. The 3D gradient and functional patterns were designed in Adobe Photoshop and converted into grayscale images. The gradient pattern was then processed through in-house software into an assembly of 11 stripe patterns adjacent to each other, and each stripe pattern was assigned a UV exposure duration based on each pattern’s stripe grayscale intensity. The gradient structure was fabricated by dynamically projecting the stripe patterns via a custom-controlled digital micromirror device (DMD) as digital optical masks projected onto the prepolymer solution. By coordinating the projection of each digital mask with the smooth movement of the prepolymer in the Z direction, photopolymerization of a series of desired focal planes results in continuous fabrication of 3D structures. The fabricated structure was then washed with 70% ethanol solution to remove any unreacted monomers.

FT-IR Characterization. FT-IR was used to characterize the thermal ring opening with polyamines, as well as the photopolymerization reactions, by monitoring the transition of functional groups such as hydroxyl, carbonyl, and alkene by FT-IR. The spectra of samples were obtained in region of 500–4000 cm^{-1} using a Spectrum Two spectrometer (PerkinElmer). An air background spectrum was collected before analysis of the sample and subtracted from each sample spectrum. The FT-IR spectrum of gPU-1, gPU-2, and gPU-3 are available in the [Supporting Information](#) (Figure S1–S3).

DSC Characterization. A differential scanning calorimeter (DSC) was used to analyze the thermal properties and structural information on the gPUs. DSC was carried out using a DSC Q20 (TA Instrument) DSC12E over a temperature range from -10 to 200 °C, increasing 10 °C/min under nitrogen.

UV–vis Characterization. Optical absorbance was measured from 350 to 1000 nm using a UV–vis spectrophotometer (Infinite 200 Pro, Tecan, Männedorf, Schweiz). To prepare gPU samples, diurethane solutions were prepared as described previously from the reaction of TMPMAC with diamine compounds such as putrescine, cadaverine, spermidine, and spermine. The resulting solutions were placed within a covered PDMS compartment with a height of 500 μm . The gPU structures were UV photopolymerized using a portable UV lamp at 350 nm. The resulting gPU scaffolds were placed in a 48-well polystyrene plate and measured. A blank was used as a control.

Scheme 1. (1) Schematic View of Green Chemistry and Optical Printing Process; (2) Synthesis Pathway of Reactions^a

^a(A) Thermal ring-opening reaction of TMPMAC with biogenic polyamines to diurethane monomers functionalized with methacrylate. (B) UV-induced polymerization of the diurethane monomers on the methacrylate group to polyurethanes.

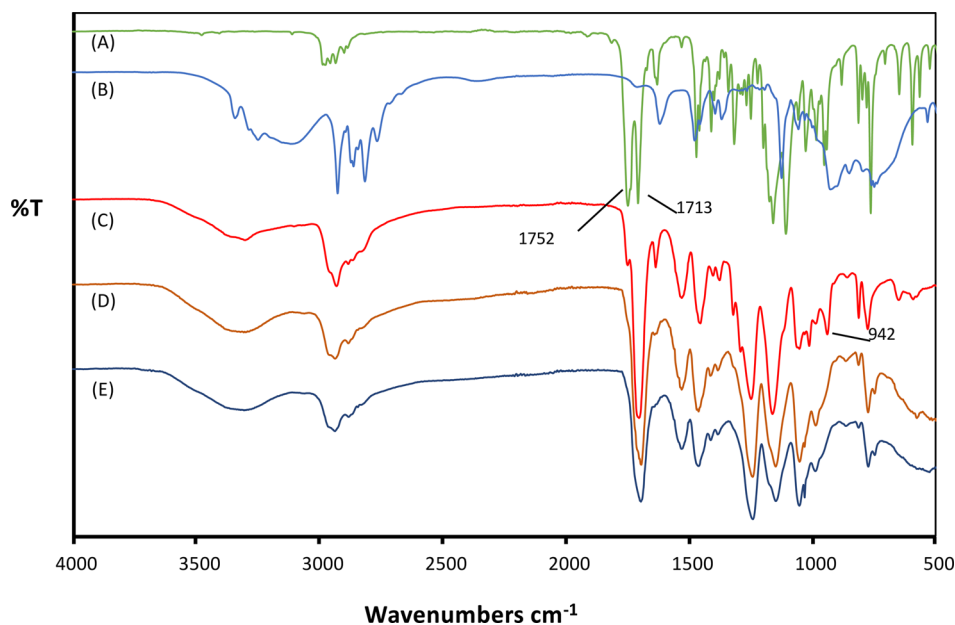


Figure 1. Representative FT-IR spectrum for polyurethanes with different preparation processes: (A) TMPMAC, (B) spermine, (C) diurethane prepared from TMPMAC and spermine by thermal reaction, (D) polyurethane cross-linked on methacrylate from diurethane by UV curing for 20 s, and (E) polyurethane cross-linked on methacrylate from diurethane by UV curing for 30 s.

Stiffness Characterization. The stiffness of the PU samples was measured by a dynamic mechanical analysis (DMA) machine (DMA 8000, PerkinElmer) and atomic force microscopy (AFM; Dimension Icon, Bruker) as described previously.⁴³ Briefly, a cone-shaped probe, 0.12 N m^{-1} spring constant with a half angle of 35° (DNP-S, Veeco), was used to indent every stripe of the substrates with a gradient of stiffness. The indentation velocity of the probe was fixed at $2 \mu\text{m/s}$, with a trigger force of 2 nN. The force volume maps were determined by the Sneddon model with a Poisson ratio of 0.5.⁴⁴ High-resolution

scanning electron microscopy (SEM) images were obtained using Philips XL30 ESEM. The surface of the structure was coated by a thin layer of iridium by an Emitech K575X Sputter Coater prior to imaging.

Cell Culture. C3H/10T1/2 cells (mouse fibroblast cell line) were maintained in Dulbecco's Modified Eagle Medium (DMEM, Gibco Life Technologies) supplemented with 10% v/v FBS (fetal bovine serum, Life Technologies), 1% penicillin/streptomycin solution (Penstrep) (Gibco Life Technologies).

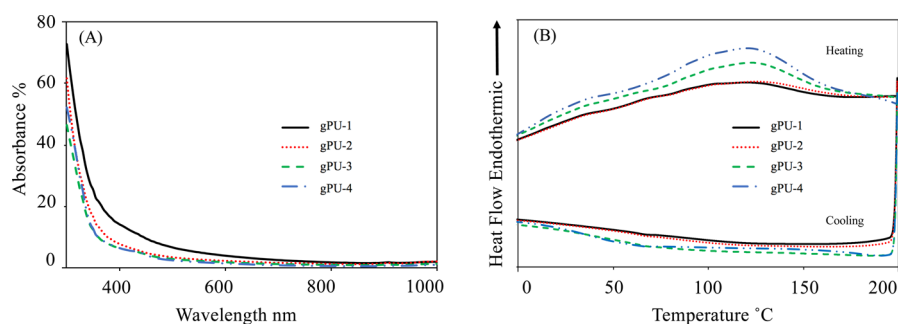


Figure 2. (A) Optical transparency of resulting polyurethanes measured by a UV-vis spectrophotometer, and (B) thermal properties measured by DSC. Polyurethanes prepared from TMPMAC and putrescine (gPU-1), cadaverine (gPU-2), spermidine (gPU-3), and spermine (gPU-4).

Cell Viability Assay. 10T1/2 cells were obtained at passage 4 and used at passages 5–8. The gPUs were printed into round shapes with a diameter of 2.5 mm, put into 24-well culture plates, and immersed in PBS with 1% Penstrep 2 days prior to seeding. The cells were seeded onto the gPU disks with a density of 100k cells/mL growth media per well. After 3 and 7 days of culturing, the samples were washed thoroughly with PBS, and a solution of calcein AM and ethidium homodimer-1 (EthD-1) (Biotium) in PBS was added to the sample per the manufacturer's protocol. The samples were incubated for 30 min at room temperature on an orbital shaker, and cell viability was assessed by fluorescence microscopy. Cells seeded on the gPUs were scanned, and the cells were counted using ImageJ.

3. RESULTS AND DISCUSSION

3.1. Preparation and Fabrication of Green Aliphatic Polyurethanes. The gPUs were prepared from a cyclic carbonate, trimethylolpropane methacrylate carbonate (TMPMAC), and polyamines. The overall reaction consists of (A) thermal formation of diurethane monomers and (B) UV-induced cross-linking polymerization (Scheme 1). More specifically, ROP of cyclic carbonates with biogenic polyamines was used to produce functional diurethane monomers. The resulting functionalized diurethanes were polymerized by free radical polymerization of the methacrylate group to form cross-linked gPUs. As shown in Scheme 1, these reactions were done in a green manner using only heat and light, thus avoiding the use of toxic isocyanates and phosgene. Four different polyamines, putrescine, cadaverine (diamine), spermidine (triamine), and spermine (tetra-amine), were chosen to investigate how their differences in chemical structure can affect PU properties—these differ in their linear backbone structure in terms of chain length and number of amine groups, and as such our gPU variants are labeled gPU-1, gPU-2, gPU-3, and gPU-4, respectively. These polyamines are natural products formed by the decarboxylation of amino acids as part of the normal metabolism of microorganisms, plants, and animals—they are also present in a wide range of foods, including dairy products and fermented foods, and can accumulate in high concentrations (e.g., >1000 mg per kilogram of cheese).^{34–36} In the second phase of our work, the resulting functionalized diurethane monomers were 3D printed via UV-based free radical polymerization of the methacrylate group to form cross-linked gPUs in user-defined geometries and material properties.

The reactants, products, and reactions between cyclic carbonates and polyamines were monitored by the transformation of functional groups using Fourier transform infrared spectroscopy (FT-IR) (Figure 1). In the first step of ROP production of functional diurethane, the 1752 cm^{-1} carbonyl group peak disappeared and merged with the 1713 cm^{-1} carbonyl peak of the methacrylate group while a new broad

peak at 3000–3500 cm^{-1} appeared, which was attributed to the ROP formation of new hydroxyl groups (Figure 1C). The reaction was measured via FT-IR over the course of 10 min and completed without solvents and catalysts. During the second step where functional diurethane monomers are UV photopolymerized, the 942 cm^{-1} peak associated with the C–H bond of monosubstituted alkene in the methacrylate group (Figure 1C) disappeared as the UV photopolymerization induced new C–C bond formations (Figure 1D). This process provides a novel, facile, and more environmentally friendly approach for synthesis of aliphatic PUs without using hazardous raw materials.

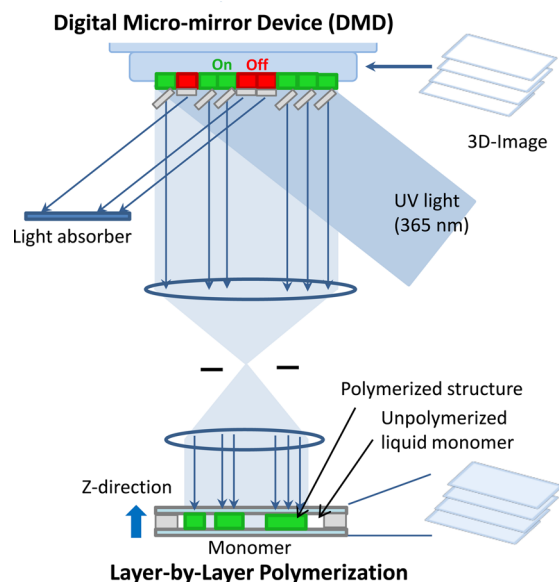
3.2. Optical and Thermal Properties of Green Aliphatic Polyurethanes. Since the COP system uses light-assisted polymerization to 3D print, the building material's optical transparency is crucial for the continuous printing of gPUs. Optical properties and transparency of our four gPU variants (gPU-1, gPU-2, gPU-3, gPU-4) were characterized by UV-vis spectrometry (Figure 2A). Within the range of measurement (350–1000 nm), the absorbance of all 4 compositions stays below 26% compared with control (blank). The absorbance of gPU-1 is slightly higher than that of the other three gPUs. At longer wavelengths, a rapid drop in absorbance (below 5% from 550 to 1000 nm) was observed for all gPUs. The absorbance for gPUs-1, gPU-2, and gPU-3 reached below 10%, while gPU-1 was about 20% at 365 nm, which is the wavelength of the UV light for 3D printing. Low absorbance at this wavelength ensures that incoming light can pass through the gPU to excite the photoinitiators, and these results indicate that all four gPU variants show good optical transparency. The high transparency and low absorbance of these biogenic gPU materials indicate that they can be directly photopolymerized into complex shapes using our continuous optical 3D printing system. Furthermore, the UV-vis data from the 360–700 nm region also indicate that the gPUs will not negatively affect fluorescence imaging experiments such as immunochemical staining and cell morphology observations.

To further study the internal structure and thermal properties of our gPUs, the printed structures were analyzed by DSC to evaluate their crystallinity and glass transition temperature (T_g). The lack of any abrupt changes in energy flow in both heating and cooling conditions demonstrates the gPU's lack of crystallinity. Additionally, DSC also showed that the gPUs did not undergo thermal decomposition or oxidation even at temperatures as high as 200 °C. This thermal stability at high temperatures allows gPU to undergo autoclave sterilization, which is a commonly used technique for prepping biomedical implants and other in vivo interactions. Future work

will include other thermal property characterizations, such as thermal expansion and thermal transition coefficient.

3.3. Continuous 3D Printing of gPUs. To demonstrate gPU printability, we utilized our custom-designed COP 3D printing system (Scheme 2), which employs a digital micro-

Scheme 2. Schematic of the Continuous Optical Printing (COP) System^a



^aUV light (365 nm) illuminates the DMD system, which generates an optical pattern according to the 3D image flow from the control computer. A 3D scaffold is printed in a layer-by-layer fashion onto the photocurable monomer by the optical pattern projected through an optical lens.

mirror array device (DMD) and projection optics to project patterned UV light onto the diurethane prepolymer solution. Via a computer interface coupled with in-house-developed software, optical patterns are automatically and dynamically loaded onto the DMD chip. Cross-linking occurs at illuminated areas rapidly, while unilluminated regions are left un-cross-linked, thus forming an image in a specific polymerization plane. This process is dynamically repeated through a series of user-defined digital masks while the stage is translated in the Z direction to precisely construct the desired 3D structure. The COP printing platform “prints” the 2D images without moving nozzles or stage in both X and Y directions and creates the 3D object continuously in the Z direction. As a result, the printing speed of COP is much faster as compared to traditional nozzle-based 3D printers. Due to the continuous movement of the stage, the fabricated 3D structures do not exhibit the planar artifacts (interfaces) induced by traditional layer-by-layer fabrication approaches that involve discrete movements of the linear stage. These existing 3D printing approaches produce structures with step-like artifacts along the Z direction due to the drop-by-drop and layer-by-layer fabrication process. The rasterless and continuous nature of the COP platform will not yield such artificial interfaces and therefore will produce a whole 3D structure with smooth contours, significantly improving the structural integrity of the printed structure. This printing platform can create not only complex polymer scaffolds but also cell-laden constructs^{43,45–47} for both in vitro and in vivo applications such as early drug screening, tissue

regeneration, and wound healing. Previous work has demonstrated the speed, precision, and versatility of similar fabrication processes on other biomaterials such as poly(ethylene glycol) diacrylate (PEGDA) and gelatin methacrylate (GelMa).^{39,48} However, these biomaterials do not have the high durability and stiffness necessary for applications such as lab-on-a-chip devices and medical implants. Combining our 3D printing system with our newly developed gPU, we aim to solve these material requirement challenges. The thermal behavior of gPUs with different polyamines was measured by repeated DSC cycles and showed similar behavior, which was almost featureless within the experimental temperature range due to cross-linking of the methacrylate group upon UV polymerization (Figure 2B).

3.4. Tunable Mechanical Properties of gPU via Optical Printing. The relation between printing parameters such as exposure time and surface stiffness of printed structures was investigated. Surface stiffness plays an important role in biomedical research.⁴⁹ To investigate how to tune the mechanical property of printed structure, we used the equation developed by Askadskii et al. to describe the elastic modulus of a polymer and its number of repeating units via the following equation^{50,51}

$$E_n = \frac{3dRT(m + \beta)}{M_0 m^2}$$

where d is the polymer density, R is the universal gas constant, T is the temperature for which the modulus was calculated, M_0 is the molecular mass of the repeat unit of the linear network fragment, m is the number of the repeat units in a linear fragment between neighboring cross-links, and β is the ratio between the an der Waals volume of the cross-link over that of the repeated unit. In the case of linear polymerization, β equals to zero.

Previously, Decker et al. computed the relation between the kinetic chain length during polymerization and the UV exposure time. Briefly, the kinetic chain length (KCL) was calculated by dividing the rate of polymerization by the rate of initiation, which is a function of both the monomer concentration and the quantum yield. The quantum yield of the polymerization is essentially a function of the exposure time, as shown in the following equations.⁵¹

Rate of polymerization

$$R_p = \frac{k_p}{(2k_t)^{0.5}} [M] r_i^{0.5}$$

Rate of initiation

$$r_i = \Phi_i \cdot I_a$$

Kinetic chain length

$$\text{KCL} = \frac{R_p}{r_i} = \frac{k_p [M] \Phi_i^{0.5}}{(2k_t)^{0.5} I_a^{0.5}}$$

Quantum yield

$$\Phi_i = \frac{[M] \times l}{f \times 1000 \times t_e \times I_a}$$

where $[M]$ is the concentration of urethane monomer, k_p is the propagation rate, k_t is the termination rate, I_a is the light intensity absorbed, l is the thickness of the printed structure, f is the fraction on incident light absorbed by the sample, and t_e is

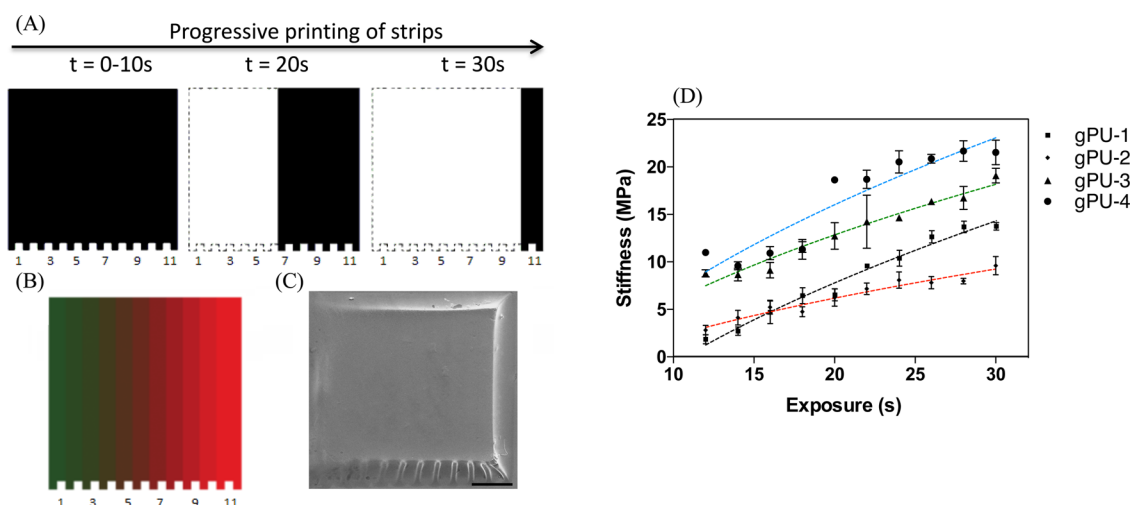


Figure 3. Optical printing of gradient pattern using gPUs by the COP system. (A) Progressive printing of strips based on the program of exposure time. (B) Designed pattern for gradient printing. (C) SEM image of printed pattern (scale bar 500 μm). (D) Stiffness of printed scaffolds prepared from putrescine (■), cadaverine (◆), spermine (▲), and spermidine (●).

the exposure time. The number of repeat units in a linear fragment between neighboring cross-links is a linear function of kinetic chain length of the polymerization. Therefore, two equations could be combined to yield the following equation

$$E_n = A \cdot \frac{d(2k_t)^{0.5} t_c^{0.5}}{M_0 k_p [M]^{1.5}}$$

For polyurethanes made by the same reactants, the polymer density, molecular weight of the repeating unit, reaction kinetics, and monomer concentration are the same. The equation could be further simplified into a square root function of exposure time. On the basis of the equation, we predicted that the stiffness of the printed structure increases with increasing exposure time. To prove this relation, we printed a structure using the COP system (Scheme 2). To investigate the parameters for printing and testing, we first printed a square shape using gPUs and tested its mechanical properties by DMA, where the results showed that the gPUs had a compression modulus of 10–24 MPa (Figure S5). The structure is made up by a series of stripes with increasing exposure time, as shown in Figure 3A. Here, a shape with increasing grayscale intensity was first designed in Adobe Photoshop. This image file was further processed by in-house software to divide it into 11 stripe patterns according to grayscale intensities as shown in Figure 3B. Each stripe pattern was associated with a specific exposure time, running from 12 to 30 s with an increment of 2 s per stripe. During the printing, the entire block was initially projected onto the monomer solution, followed by disappearance of the stripe pattern from one end to another until all stripes disappeared (Figure 3A). A structure with increasing exposure time was obtained and imaged by SEM (Figure 3C). The stiffness of each stripe was measured by AFM after soaking in ethanol and air dried. As expected, the results follow a square root function of the exposure times (Figure 3D). The structures and the number of amines in the polyamine linkers also affect the stiffness of the polymer created as indicated by the AFM data. Between gPU-1 and gPU-2, which were prepared from diamines of straight 4-carbones (putrescine) and 5-carbones (cadaverine), respectively, the higher stiffness gPU was prepared from shorter compounds due to the lower chain flexibility. However, gPU-3

and gPU-4 exhibited higher stiffness, as they were prepared from triamine (spermidine) and tetra-amine (spermine), which have longer chain lengths than the amines used in gPU-1 and gPU-2. This behavior can also be explained by partial participation of secondary amines inside the chain in the formation of diurethane. Additionally, since the decreasing number of repeating units between cross-links has a higher impact on the resultant elasticity, this can compensate for the increase of molecular weight of the monomer. Overall gPU stiffness was tunable by controlling the exposure time and by selecting different polyamine compounds, and we anticipate that in future works these tunable stiffness gradient patterns can be used for the study of cell motion and differentiation.

3.5. Structures Featuring Curves and Complex Contours by 3D Printing. Curves and complex contours on the surface are essential in 3D printing of biology relevant and intrinsic structures. To demonstrate rapid 3D printing with the gPUs via our COP system, a complex gradient design was created and processed into a series of transverse planes according to the grayscale of each pixel, as shown in Figure 4A. These planes were projected onto the monomer solution. During the printing process, the stage constantly moves upward to project the patterns from bottom to top within the monomer solution (Figure 4B and 4C). When the stage moves to a slightly higher location, a different pattern is projected and covalently bonded with the previous pattern in the stack. Thus, a structure with complex surface contour can be fabricated through a series of planar patterns stacking on top of each other. Figure 4D and 4E demonstrates a complex printed structure which resembles the contour outline of a shark scale. Shark skin possesses small features called placoid scales, and they have unique hydrodynamic, antifouling, and bacterial repulsion properties.^{52–54} Fabricating biomimetically derived complex surface contours is of interest to the scientific community but has been challenging for rapid prototyping techniques such as nozzle-based or inkjet printing. With such techniques, the intermittent motion of the dispensing system relative to the deposited material often creates defects between connected layers. However, in our COP system, each layer is created smoothly and continuously on top of previous layers, eliminating such defects and enabling us to quickly (~ 30 s)

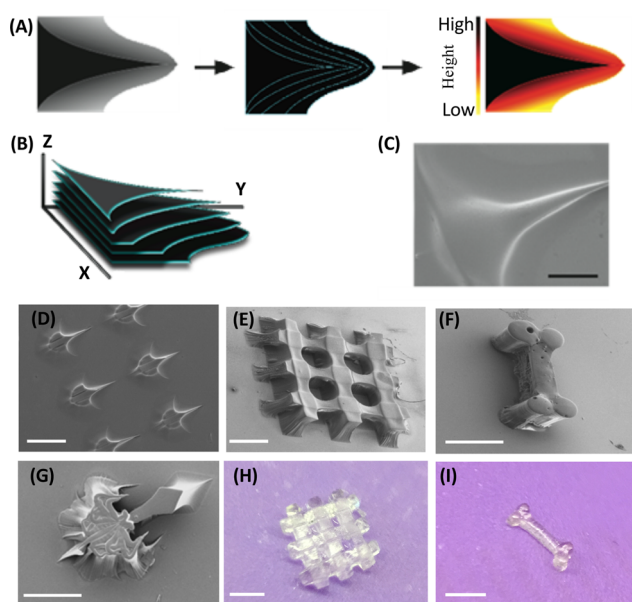


Figure 4. Optical printing of intricate structures using gPUs by the COP system. (A) Schematic process showing software-aided 3D reconstruction from grayscale patterns. (B) Layer-by-layer printing procedure of 3D structure guided by computer. (C) SEM image of printed pattern (gPU-4). (D) Complex contour biomimetic structures of shark skin. (E–I) Complex contour functional structures of log-pile, squid, and bone. Scale bars: (C) 200 and (D–I) 500 μm . See the Supporting Information (Figure S4) for SEM images of gPU-1, gPU-2, gPU-3, and gPU-4.

print a complex sharkskin scale structure with smooth surface contours and a biomimetic double-bump surface pattern. Furthermore, the images of Figure 4C–I showcase other 3D-printed structures, such as a log-pile, a dog bone, and squids, all of which have applications in soft robotics, microfluidics, and biomedical research.⁵⁵ gPU's optical and mechanical properties make it an excellent material choice for printing structures with high fidelity, complexity, and smoothness.

3.6. Biocompatibility of gPU Materials. The green chemistry process used in this work does away with hazardous reagents, and the overall reaction does not include any cytotoxic materials. Additionally, the similarity in chemical structure between urethane functional groups and amino acids raises a question in whether this material could be used without surface modifications for cell culture applications, as the urethane groups can function as potential cell binding sites. To further explore gPU's potential in biomedical research, we investigated the cytocompatibility of C3H 10T1/2 cells seeded directly on the printed structures (Figure 5). This type of fibroblast cell is widely used as a model cell in many biology studies, especially in toxicity screening and tissue engineering.⁵⁶ gPU was printed into round shapes with diameters of 2.5 mm, put into 24-well culture plates, and immersed in PBS with 1% penicillin streptomycin 2 days prior to seeding. The 10T1/2 cells were obtained at passage 4, used at passages 5–8, and maintained in DMEM growth media with 10% FBS. The cells were seeded onto gPU structures at a density of 100k cells/mL growth media per well. After 3 and 7 days of incubation, cell viabilities were measured using calcein AM and ethidium homodimer assays according to the manufacturer's instructions. High cell viability (over 95%) for each material was obtained (Figure 5). Both the morphology and the high viability of the

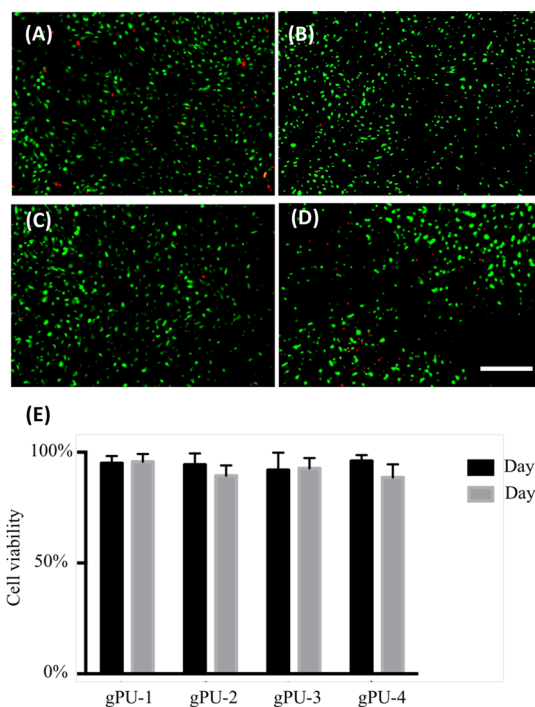


Figure 5. Immunostaining to examine cell viability after seeded on (A) gPU-4 at day 3, (B) gPU-4 at day 7, (C) culture plate (control) at day 3, and (D) at day 7. Cells seeded on all 4 gPUs have more than 95% cell viability after 3 and 7 days' postseeding. Scale bar = 200 μm .

cells suggested that gPUs are a viable material choice for biomedical applications.

4. CONCLUSIONS

In conclusion, we report the continuous optical 3D printing of a photopolymerizable, isocyanate-free PU. We demonstrate the rapid printing of tunable stiffness gradients and smooth contours in 3D-printed structures of biomimetic design as well as characterizing their optical and mechanical properties. Our green chemistry synthesis approach in combining various cyclic carbonates with polyamines allows for unique tailoring of gPU physicochemical properties and our custom continuous optical printing technology can enable the fabrication of user-defined properties and 3D structural features. We anticipate that our isocyanate-free gPU materials will help satisfy critical safety issues in biomedical and consumer products and that our 3D-printed gPU devices can be applied across broader applications, such as mechanically durable medical implants, tissue engineering scaffolds, microfluidic devices, diagnostic probes, and lab-on-a-chip systems.

■ ASSOCIATED CONTENT

Supporting Information

The Supporting Information is available free of charge on the ACS Publications website at DOI: 10.1021/acsami.6b12500.

FT-IR spectrum for the preparation process of isocyanate-free polyurethane (gPU-1), FT-IR spectrum for the preparation process of isocyanate-free polyurethane (gPU-2), FT-IR spectrum for the preparation process of isocyanate-free polyurethane (gPU-3), SEM images of 3D-printed biomimicking structures using isocyanate-free polyurethanes, and compressive modulus

of gPU-4 measured by DMA using frequency scan (PDF)

AUTHOR INFORMATION

Corresponding Author

*E-mail: chen168@eng.ucsd.edu.

ORCID

Pengrui Wang: 0000-0001-9185-2951

Author Contributions

[†]S.-H.P. and P.W. contributed equally to this work.

Notes

The authors declare no competing financial interest.

ACKNOWLEDGMENTS

The work was supported by VINNOVA (The Swedish Agency for Innovation System) and Swedish Research Council Formas to S.-H.P. and grants from the Department of Defense (W81XWH-14-1-0522), California Institute for Regenerative Medicine (RT3-07899), and National Science Foundation (CMMI-1332681 and CMMI-1644967) to S.C. The authors thank Dr. Nathan Gianneschi for providing the AFM for measurements.

REFERENCES

- (1) Phan, T. V. T.; Gallardo, C.; Mane, J. *Green Chem.* **2015**, *17*, 2846–2852.
- (2) Chen, F. M.; Liu, X. Advancing Biomaterials of Human Origin for Tissue Engineering. *Prog. Polym. Sci.* **2016**, *53*, 86–168.
- (3) Ravichandran, R.; Sundarajan, S.; Venugopal, J. R.; Mukherjee, S.; Ramakrishna, S. Advances in Polymeric Systems for Tissue Engineering and Biomedical Applications. *Macromol. Biosci.* **2012**, *12* (3), 286–311.
- (4) Cha, C.; Soman, P.; Zhu, W.; Nikkhah, M.; Camci-Unal, G.; Chen, S.; Khademhosseini, A. Structural Reinforcement of Cell-Laden Hydrogels with Microfabricated Three Dimensional Scaffolds. *Biomater. Sci.* **2014**, *2* (5), 703–709.
- (5) Kucinska-Lipka, J.; Gubanska, I.; Janik, H.; Sienkiewicz, M. Fabrication of Polyurethane and Polyurethane Based Composite Fibres by the Electrospinning Technique for Soft Tissue Engineering of Cardiovascular System. *Mater. Sci. Eng., C* **2015**, *46*, 166–176.
- (6) Li, X.; Wang, L.; Fan, Y.; Feng, Q.; Cui, F. Z.; Watari, F. Nanostructured Scaffolds for Bone Tissue Engineering. *J. Biomed. Mater. Res., Part A* **2013**, *101A* (8), 2424–2435.
- (7) Zhong, C.; Wu, J.; Reinhart-King, C. A.; Chu, C. C. Synthesis, Characterization and Cytotoxicity of Photo-Crosslinked Maleic Chitosan-Polyethylene Glycol Diacrylate Hybrid Hydrogels. *Acta Biomater.* **2010**, *6* (10), 3908–3918.
- (8) Eglin, D.; Mortisen, D.; Alini, M. Degradation of Synthetic Polymeric Scaffolds for Bone and Cartilage Tissue Repairs. *Soft Matter* **2009**, *5* (5), 938.
- (9) Chang, P.-C.; Liu, B.-Y.; Liu, C.-M.; Chou, H.-H.; Ho, M.-H.; Liu, H.-C.; Wang, D.-M.; Hou, L.-T. Bone Tissue Engineering with Novel rhBMP2-PLLA Composite Scaffolds. *J. Biomed. Mater. Res., Part A* **2007**, *81A* (4), 771–780.
- (10) Singhal, P.; Small, W.; Cosgriff-Hernandez, E.; Maitland, D. J.; Wilson, T. S. Low Density Biodegradable Shape Memory Polyurethane Foams for Embolic Biomedical Applications. *Acta Biomater.* **2014**, *10* (1), 67–76.
- (11) Stevenson, A. T.; Reese, L. M.; Hill, T. K.; McGuire, J.; Mohs, A. M.; Shekhar, R.; Bickford, L. R.; Whittington, A. R. Fabrication and Characterization of Medical Grade Polyurethane Composite Catheters for near-Infrared Imaging. *Biomaterials* **2015**, *54*, 168–176.
- (12) Chen, Q.; Liang, S.; Thouas, G. A. Elastomeric Biomaterials for Tissue Engineering. *Prog. Polym. Sci.* **2013**, *38* (3–4), 584–671.
- (13) Bezwada, R. S. U.S. Patent. 8,846,845, 2014.
- (14) Heederik, D.; Henneberger, P. K.; Redlich, C. A. Primary Prevention: Exposure Reduction, Skin Exposure and Respiratory Protection. *Eur. Respir. Rev.* **2012**, *21* (124), 112–124.
- (15) Vermette, P.; Griesser, H. J.; Laroche, G.; Guidoin, R. *Biomedical Applications of Polyurethanes*; Landes Bioscience: Georgetown, TX, 2001.
- (16) Lockey, J. E.; Dunning, K.; Hilbert, T. J.; Borton, E.; Levin, L.; Rice, C. H.; McKay, R. T.; Shipley, R.; Meyer, C. A.; Perme, C.; LeMasters, G. K. HRCT/CT and Associated Spirometric Effects of Low Libby Amphibole Asbestos Exposure. *J. Occup. Environ. Med.* **2015**, *57* (1), 6–13.
- (17) Panwar, H.; Raghuram, G. V.; Jain, D.; Ahirwar, A. K.; Khan, S.; Jain, S. K.; Pathak, N.; Banerjee, S.; Maudar, K. K.; Mishra, P. K. Cell Cycle Deregulation by Methyl Isocyanate: Implications in Liver Carcinogenesis. *Environ. Toxicol.* **2014**, *29* (3), 284–297.
- (18) Pyo, S.-H.; Persson, P.; Mollaahmad, M. A.; Sørensen, K.; Lundmark, S.; Hatti-Kaul, R. Cyclic Carbonates as Monomers for Phosgene- and Isocyanate-Free Polyurethanes and Polycarbonates. *Pure Appl. Chem.* **2011**, *84* (3), 637–661.
- (19) Guelcher, S. A.; Srinivasan, A.; Dumas, J. E.; Didier, J. E.; McBride, S.; Hollinger, J. O. Synthesis, Mechanical Properties, Biocompatibility, and Biodegradation of Polyurethane Networks from Lysine Polyisocyanates. *Biomaterials* **2008**, *29* (12), 1762–1775.
- (20) Chapin, R. E.; Adams, J.; Boekelheide, K.; Gray, L. E.; Hayward, S. W.; Lees, P. S. J.; McIntyre, B. S.; Portier, K. M.; Schnorr, T. M.; Selevan, S. G.; Vandenberg, J. G.; Woskie, S. R.; Shelby, M. D. NTP-CERHR Expert Panel Report on the Reproductive and Developmental Toxicity of Bisphenol A. *Birth Defects Res., Part B* **2008**, *83* (3), 157–395.
- (21) Kreye, O.; Mutlu, H.; Meier, M. a. R. Sustainable Routes to Polyurethane Precursors. *Green Chem.* **2013**, *15* (6), 1431–1455.
- (22) Kathalewar, M. S.; Joshi, P. B.; Sabnis, A. S.; Malshe, V. C. Non-Isocyanate Polyurethanes: From Chemistry to Applications. *RSC Adv.* **2013**, *3* (13), 4110.
- (23) Anastas, P. T.; Warner, J. C. *Green Chemistry: Theory and Practice*; Oxford University Press: New York, 1998.
- (24) Holbrey, J. D.; Reichert, W. M.; Swatoski, R. P.; Broker, G. A.; Pitner, W. R.; Seddon, K. R.; Rogers, R. D. Efficient, Halide Free Synthesis of New, Low Cost Ionic Liquids: 1,3-Dialkylimidazolium Salts Containing Methyl- and Ethyl-Sulfate Anions. *Green Chem.* **2002**, *4* (5), 407–413.
- (25) Kumaravel, K.; Vasuki, G. Four-Component Catalyst-Free Reaction in Water: Combinatorial Library Synthesis of Novel 2-Amino-4-(5-Hydroxy-3-Methyl-1H-Pyrazol-4-Yl)-4H-Chromene-3-Carbonitrile Derivatives. *Green Chem.* **2009**, *11* (12), 1945.
- (26) Loupy, A. Solvent-Free Microwave Organic Synthesis as an Efficient Procedure for Green Chemistry. *C. R. Chim.* **2004**, *7* (2), 103–112.
- (27) Lombardo, V. M.; Dhulst, E. A.; Leitsch, E. K.; Wilmot, N.; Heath, W. H.; Gies, A. P.; Miller, M. D.; Torkelson, J. M.; Scheidt, K. A. Cooperative Catalysis of Cyclic Carbonate Ring Opening: Application Towards Non-Isocyanate Polyurethane Materials. *Eur. J. Org. Chem.* **2015**, *2015* (13), 2791–2795.
- (28) Tomita, H.; Sanda, F.; Endo, T. Structural Analysis of Polyhydroxyurethane Obtained by Polyaddition of Bifunctional Five-Membered Cyclic Carbonate and Diamine Based on the Model Reaction. *J. Polym. Sci., Part A: Polym. Chem.* **2001**, *39* (6), 851–859.
- (29) Pyo, S. H.; Hatti-Kaul, R. Selective, Green Synthesis of Six-Membered Cyclic Carbonates by Lipase-Catalyzed Chemospecific Transesterification of Diols with Dimethyl Carbonate. *Adv. Synth. Catal.* **2012**, *354* (5), 797–802.
- (30) Pyo, S.-H.; Hatti-Kaul, R. Chlorine-Free Synthesis of Organic Alkyl Carbonates and Five- and Six-Membered Cyclic Carbonates. *Adv. Synth. Catal.* **2016**, *358* (5), 834–839.
- (31) Rokicki, G. Aliphatic Cyclic Carbonates and Spiroorthocarbonates as Monomers. *Prog. Polym. Sci.* **2000**, *25* (2), 259–342.
- (32) Feng, J.; Zhuo, R. X.; Zhang, X. Z. Construction of Functional Aliphatic Polycarbonates for Biomedical Applications. *Prog. Polym. Sci.* **2012**, *37* (2), 211–236.

- (33) Mespouille, L.; Coulembier, O.; Kawalec, M.; Dove, A. P.; Dubois, P. Implementation of Metal-Free Ring-Opening Polymerization in the Preparation of Aliphatic Polycarbonate Materials. *Prog. Polym. Sci.* **2014**, *39* (6), 1144–1164.
- (34) Linares, D. M.; Martín, M.; Ladero, V.; Alvarez, M. A.; Fernández, M.; Ia, M.; Andez, F. Biogenic Amines in Dairy Products. *Crit. Rev. Food Sci. Nutr.* **2011**, *51* (7), 691–703.
- (35) Spano, G.; Russo, P.; Lonvaud-Funel, a; Lucas, P.; Alexandre, H.; Grandvalet, C.; Coton, E.; Coton, M.; Barnavon, L.; Bach, B.; Rattray, F.; Bunte, a; Magni, C.; Ladero, V.; Alvarez, M.; Fernández, M.; Lopez, P.; de Palencia, P. F.; Corbi, a; Trip, H.; Lolkema, J. S. Biogenic Amines in Fermented Foods. *Eur. J. Clin. Nutr.* **2010**, *64*, S95–S100.
- (36) Ladero, V.; Calles-Enriquez, M.; Fernandez, M.; Alvarez, M. A. Toxicological Effects of Dietary Biogenic Amines. *Curr. Nutr. Food Sci.* **2010**, *6* (2), 145–156.
- (37) Park, J.; Tahk, D.; Ahn, C.; Im, S. G.; Choi, S.-J.; Suh, K.-Y.; Jeon, S. Conformal Phase Masks Made of Polyurethane Acrylate with Optimized Elastic Modulus for 3D Nanopatterning. *J. Mater. Chem. C* **2014**, *2* (13), 2316.
- (38) Hsieh, F. Y.; Lin, H. H.; Hsu, S. hui. 3D Bioprinting of Neural Stem Cell-Laden Thermoresponsive Biodegradable Polyurethane Hydrogel and Potential in Central Nervous System Repair. *Biomaterials* **2015**, *71*, 48–57.
- (39) Zhu, W.; Li, J.; Leong, Y. J.; Rozen, I.; Qu, X.; Dong, R.; Wu, Z.; Gao, W.; Chung, P. H.; Wang, J.; Chen, S. 3D-Printed Artificial Microfish. *Adv. Mater.* **2015**, *27* (30), 4411–4417.
- (40) Tumbleston, J. R.; Shirvanyants, D.; Ermoshkin, N.; Januszewicz, R.; Johnson, A. R.; Kelly, D.; Chen, K.; Pinschmidt, R.; Rolland, J. P.; Ermoshkin, A.; Samulski, E. T.; DeSimone, J. M. Continuous Liquid Interface Production of 3D Objects. *Science (Washington, DC, U. S.)* **2015**, *347* (6228), 1349–1352.
- (41) National Toxicology Program. Toxicology and Carcinogenesis Studies of Trimethylolpropane Triacrylate (Technical Grade) (CASRN 15625-89-5) in F344/N Rats and B6C3F1/N Mice (Dermal Studies). *Natl. Toxicol. Program Tech. Rep. Ser.* **2012**, No. 576, 1–144.
- (42) Qu, X.; Zhu, W.; Huang, S.; Li, Y. S.; Chien, S.; Zhang, K.; Chen, S. Relative Impact of Uniaxial Alignment vs. Form-Induced Stress on Differentiation of Human Adipose Derived Stem Cells. *Biomaterials* **2013**, *34* (38), 9812–9818.
- (43) Hribar, K. C.; Finlay, D.; Ma, X.; Qu, X.; Ondeck, M. G.; Chung, P. H.; Zanella, F.; Engler, A. J.; Sheikh, F.; Vuori, K.; Chen, S. C. Nonlinear 3D Projection Printing of Concave Hydrogel Microstructures for Long-Term Multicellular Spheroid and Embryoid Body Culture. *Lab Chip* **2015**, *15* (11), 2412–2418.
- (44) Chang, Y. R.; Raghunathan, V. K.; Garland, S. P.; Morgan, J. T.; Russell, P.; Murphy, C. J. Automated AFM Force Curve Analysis for Determining Elastic Modulus of Biomaterials and Biological Samples. *J. Mech. Behav. Biomed. Mater.* **2014**, *37*, 209–218.
- (45) Lu, Y.; Mapili, G.; Suhali, G.; Chen, S.; Roy, K. A Digital Micro-mirror Device-based System for the Microfabrication of Complex, Spatially Patterned Tissue Engineering Scaffolds. *J. Biomed. Mater. Res., Part A* **2006**, *77A* (2), 396–405.
- (46) Grogan, S. P.; Chung, P. H.; Soman, P.; Chen, P.; Lotz, M. K.; Chen, S.; D'Lima, D. D. Digital Micromirror Device Projection Printing System for Meniscus Tissue Engineering. *Acta Biomater.* **2013**, *9* (7), 7218–7226.
- (47) Soman, P.; Chung, P. H.; Zhang, A. P.; Chen, S. Digital Microfabrication of User-Defined 3D Microstructures in Cell-Laden Hydrogels. *Biotechnol. Bioeng.* **2013**, *110* (11), 3038–3047.
- (48) Hribar, K. C.; Choi, Y. S.; Ondeck, M.; Engler, A. J.; Chen, S. Digital Plasmonic Patterning for Localized Tuning of Hydrogel Stiffness. *Adv. Funct. Mater.* **2014**, *24* (31), 4922–4926.
- (49) Rape, A. D.; Zibinsky, M.; Murthy, N.; Kumar, S. A Synthetic Hydrogel for the High-Throughput Study of Cell-ECM Interactions. *Nat. Commun.* **2015**, *6* (May), 8129.
- (50) Askadskii, A. A. Influence of Crosslinking Density on the Properties of Polymer Networks. *Polym. Sci. U.S.S.R.* **1990**, *32* (10), 2061–2069.
- (51) Decker, C. Kinetic Study and New Applications of UV Radiation Curing. *Macromol. Rapid Commun.* **2002**, *23* (18), 1067–1093.
- (52) Sakamoto, A.; Terui, Y.; Horie, C.; Fukui, T.; Masuzawa, T.; Sugawara, S.; Shigeta, K.; Shigeta, T.; Igarashi, K.; Kashiwagi, K. Antibacterial Effects of Protruding and Recessed Shark Skin Micropatterned Surfaces of Polyacrylate Plate with a Shallow Groove. *FEMS Microbiol. Lett.* **2014**, *361* (1), 10–16.
- (53) Oeffner, J.; Lauder, G. V. The Hydrodynamic Function of Shark Skin and Two Biomimetic Applications. *J. Exp. Biol.* **2012**, *215*, 785–795.
- (54) Kirschner, C. M.; Brennan, A. B. Bio-Inspired Antifouling Strategies. *Annu. Rev. Mater. Res.* **2012**, *42*, 211–229.
- (55) Gauvin, R.; Chen, Y.; Lee, J. W.; Soman, P.; Zorlutuna, P.; Nichol, J. W.; Bae, H.; Chen, S.; Khademhosseini, A. Biomaterials Microfabrication of Complex Porous Tissue Engineering Scaffolds Using 3D Projection Stereolithography. *Biomaterials* **2012**, *33* (15), 3824–3834.
- (56) Noushad, M.; Kannan, T. P.; Husein, A.; Abdullah, H.; Ismail, A. R. Genotoxicity Evaluation of Locally Produced Dental Porcelain - An in Vitro Study Using the Ames and Comet Assays. *Toxicol. In Vitro* **2009**, *23* (6), 1145–1150.